1-1-2018

Graphene-Oxide-Loaded Superparamagnetic Iron Oxide Nanoparticles for Ultrasensitive Electrocatalytic Detection of MicroRNA

Md Nazmul Islam
Griffith University

Lena Gorgannezhad
Griffith University

Mostafa Kamal Masud
Griffith University, University of Wollongong, mkm590@uowmail.edu.au

Shunsuke Tanaka
University of Wollongong, National Institute for Materials Science, st781@uowmail.edu.au

Md. Shahriar Al Hossain
University of Wollongong, University of Queensland, shahriar@uow.edu.au

See next page for additional authors

Graphene-Oxide-Loaded Superparamagnetic Iron Oxide Nanoparticles for Ultrasensitive Electrocatalytic Detection of MicroRNA

Abstract

We report the electrocatalytic activity of a new class of superparamagnetic nanoparticles, graphene-oxide-loaded iron oxide (GO/IO hybrid material), towards the reduction of ruthenium hexaammine(III) chloride (Ru(NH3)6]3+, RuHex). Leveraging the electrocatalytic activity of the GO/IO hybrid material and the signal enhancement capacity of [Ru(NH3)6]3+/[Fe(CN)6]3 in an electrocatalytic cycle, an ultrasensitive and specific electrochemical sensor was developed for the detection of cancerrelated microRNA (miRNA). Using the direct affinity interaction between RNA and graphene oxide, magnetically isolated and purified target miRNA were directly adsorbed onto a screenprinted electrode modified with the GO/IO hybrid material. The detection was enabled by chronocoulometric (CC) readout of charge-compensating [Ru(NH3)6]3+ followed by an enhancement in CC charge display through the Ru(NH3)6]3+ /[Fe(CN)6]3 system. We demonstrate an excellent limit of detection of 1.0 fM by accurately detecting miR-21 in synthetic samples and showcase its clinical utility in ovarian cancer cell lines with high sensitivity (ten cells) and good reproducibility (%RSD= <5%, for n=3).

Disciplines

Engineering | Physical Sciences and Mathematics

Publication Details

Islam, M., Gorgannezhad, L., Masud, M. Kamal., Tanaka, S., Hossain, M. A., Yamauchi, Y., Nguyen, N. & Shiddiky, M. J. A. (2018). Graphene-Oxide-Loaded Superparamagnetic Iron Oxide Nanoparticles for Ultrasensitive Electrocatalytic Detection of MicroRNA. ChemElectroChem, 5 (17), 2488-2495.

Authors

Md Nazmul Islam, Lena Gorgannezhad, Mostafa Kamal Masud, Shunsuke Tanaka, Md. Shahriar Al Hossain, Yusuke Yamauchi, Nam-Trung Nguyen, and Muhammad J. A Shiddiky

ChemPubSoc Europe

DOI: 10.1002/celc.201800339

CHEMELECTROCHEM Articles

Graphene-Oxide-Loaded Superparamagnetic Iron Oxide Nanoparticles for Ultrasensitive Electrocatalytic Detection of MicroRNA

Md. Nazmul Islam,[a, b] Lena Gorgannezhad,[a, b] Mostafa Kamal Masud,[b, c] Shunsuke Tanaka,[c, d] Md. Shahriar A. Hossain,*[c, e] Yusuke Yamauchi,[f, g] Nam-Trung Nguyen,[b] and Muhammad J. A. Shiddiky*[a, b]

We report the electrocatalytic activity of a new class of superparamagnetic nanoparticles, graphene-oxide-loaded iron oxide (GO/IO hybrid material), towards the reduction of ruthenium hexaammine(III) chloride ($Ru(NH_3)_6]^{3+}$, RuHex). Leveraging the electrocatalytic activity of the GO/IO hybrid material and the signal enhancement capacity of $[Ru(NH_3)_6]^{3+}/[Fe(CN)_6]^{3-}$ in an electrocatalytic cycle, an ultrasensitive and specific electrochemical sensor was developed for the detection of cancer-related microRNA (miRNA). Using the direct affinity interaction between RNA and graphene oxide, magnetically isolated and purified target miRNA were directly adsorbed onto a screen-printed electrode modified with the GO/IO hybrid material. The detection was enabled by chronocoulometric (CC) readout of charge-compensating $[Ru(NH3)_6]^{3+}$ followed by an enhancement in CC charge display through the $Ru(NH_3)_6]^{3+}/[Fe(CN)_6]^{3-}$ system. We demonstrate an excellent limit of detection of 1.0 fM by accurately detecting miR-21 in synthetic samples and showcase its clinical utility in ovarian cancer cell lines with high sensitivity (ten cells) and good reproducibility (% RSD = < 5 %, for $n = 3$).

1. Introduction

MicroRNAs (miRNAs) represent a family of short (18-25 nucleotides) and endogenous non-coding RNA species that actively regulate a range of cellular processes.[1] Dysregulated miRNA expression is directly associated with the pathogenesis of various diseases including cancer and thereby emerged as prominent diagnostic and prognostic biomarkers for these pathological conditions.[2] Despite their huge potential in diagnostics and precision medicine, biosensing of miRNAs has proven to be a considerable challenge because of their tiny size, cross interference from non-specific molecules (i.e., lack of specificity against a background of overwhelmingly abundant irrelevant molecules and non- target RNAs with sequence and size similarity), extremely low abundance (0.01 % of the bulk RNA pool, or few of molecules per cell).[3] At present, miRNA detection techniques mostly rely on conventional nucleic acid detection assays such as quantitative reverse transcription PCR (RT-qPCR), microarrays, Northern blot and RNA-sequencing.[4] Despite being reliable in laboratory settings, these conventional techniques are expensive and not suitable for the resource-poor and decentralized settings.[3,5] Few of the common pitfalls include the need for specially designed primers (e.g., hairpin or oligo-dT in qPCR), high sample volume requirements, platform-dependent variation in the analysis, assay complexity and long analysis time that may range from hours (e.g., PCR) to days (e.g., microarray).[3,5]

Biosensors-based approaches, such as electrochemical assays, on the contrary, have shown more potential for clinical application due to their inherent advantages of being inexpensive, simple, rapid, and miniaturized.[6] Most of the electrochemical sensors for miRNA however still rely on multiple sensor fabrication steps, some sorts of enzymatic amplification and target RNA modification (e.g., polyadenylation, labelling) which could destabilize RNA and complicate the assay proto-

[a] Dr. M. N. Islam, L. Gorgannezhad, Dr. M. J. A. Shiddiky
School of Environment and Science
Griffith University
Nathan Campus, QLD 4111 (Australia)
E-mail: m.shiddiky@griffith.edu.au
[b] Dr. M. N. Islam, L. Gorgannezhad, M. K. Masud, Prof. N.-T. Nguyen, Dr. M. J. A. Shiddiky
Queensland Micro- and Nanotechnology Centre
Griffith University
Nathan Campus, QLD 4111 (Australia)
[c] M. K. Masud, S. Tanaka, Dr. M. S. A. Hossain
Australian Institute for Innovative Materials (AIIM)
University of Wollongong
Squires Way, North Wollongong, NSW 2500 (Australia)
[d] S. Tanaka
International Center for Materials Nanoarchitectonics (WPI-MANA)
National Institute for Materials Science (NIMS)
1-1 Namiki, Tsukuba, Ibaraki 305-0044 (Japan)
[e] Dr. M. S. A. Hossain
School of Mechanical and Mining Engineering
The University of Queensland
Brisbane, QLD 4072 (Australia)
E-mail: md.hossain@uq.edu.au
[f] Prof. Y. Yamauchi
School of Chemical Engineering and Australian
Institute for Bioengineering and Nanotechnology (AIBN)
The University of Queensland
Brisbane, QLD 4072 (Australia)
[g] Prof. Y. Yamauchi
Department of Plant & Environmental New Resources
Kyung Hee University, 1732 Deogyeong-daero
Giheunggu, Yongin-si, Gyeonggi-do 446-701, South Korea

Supporting information for this article is available on the WWW under https://doi.org/10.1002/celc.201800339

col.[3,7] In addition, even with rigorous target selectivity and faster analysis time, many of these sensors lack additional signal enhancement steps, thereby failing to achieve the sensitivity levels required for the analysis of miRNA in clinical samples.

To enhance the sensitivity of the assays, various signal amplification strategies such as rolling circle amplification, hybridization chain reaction amplification and catalyzed hairpin assembly amplification have been incorporated in electrochemical miRNA analysis workflows. Amplification bias and longer analysis time are among the most prominent shortcomings of these signal amplification methods.[7]

An increasing number of reports, however, has indicated that the use of functional nanomaterials in electrochemical assays can prove to be an effective alternative strategy for enhancement of assay sensitivity and specificity.[8,9] Among nanomaterials, there has been a growing interest in the synthesis of magnetic transition metal oxide-based nanoparticles (NPs) due to their unique physicochemical properties such as biofavorable network structures as well as intrinsic enzyme mimetic and electrocatalytic activities.[10–16] Such metal oxides have been combined with a second nanomaterial to fabricate hybrid nanocomposites with superior functionalities resulting from the synergetic advantages of both the nanoparticles in the composites.[11] In addition to that, to meet the specific requirements of the biosensors hybrid nanomaterials have also been engineered with a variety of novel design framework, fabrication and synthesis approaches.[17] One of such effective approaches is the fabrication of porous structures in the nanocomposite which significantly enhances the functional surface area.[18] Compared to monometallic and nonporous counterparts of similar mass, these hybrid porous materials exhibit significantly improved surface functionalities (e.g., increased interaction with target analyte) and higher catalytic activities by maximizing the surface dependent mass transport.[19] Moreover, magnetic properties of these materials allow an intimate magnetic mixing and purification of target analyte which enhances the speed and specificity of the bioassays.[20] In particular, metallic iron oxide-based hybrid nanocomposites have found a wide range of potential applications owing to their unique optical, electronic, magnetic, catalytic, and sensing properties.[19,21] For example, iron oxide nanocomposite loaded with gold nanoparticles have recently been used to develop electrochemical sensors for autoantibody and microRNA.[20,22–24] Over the past several years, captivating the presence of different functional reactive moieties and exceptional physical properties at biological interfaces, graphene and graphene oxide have also been combined with iron oxide-based hybrid nanomaterials to develop electrochemical bioassays for detecting various analytes that includes NADH, H_2O_2, nitrite, uric acid, ascorbic acid, dopamine, protein and nucleic acids.[25,26]

In this paper, we show the electrocatalytic properties of a novel graphene oxide-loaded iron oxide (GO/IO hybrid) nanoparticle towards the reduction of ruthenium hexaammine(III) chloride ($Ru(NH_3)_6Cl_3$; RuHex) using typical Michaelis-Menten equation for enzyme catalysis. The morphology of GO/IO hybrid materials was engineered in such way that it obtained a highly porous structure with an improved functional surface area, which facilitated the adsorption of a significantly higher amount magnetically purified target miRNA on the GO/IO hybrid- modified sensor *via* RNA-graphene affinity interaction. The level of miRNAs was quantified by chronocoulometric (CC) charge interrogation in the presence of surface-bound cationic ruthenium hexaammine(III) chloride ($[Ru(NH_3)_6]^{3+}$) that was electrostatically attached with the anionic phosphate backbone of the adsorbed target miRNA. The signal was further enhanced with the coupling of higher amount of the ferri/ferrocyanide ($[Fe(CN)_6]^{3-/4-}$) system (i.e., $[Ru(NH3)_6]^{3+}/[Fe(CN)_6]^{3-}$ electrocatalytic cycle). The electrocatalytic reaction of $[Ru(NH_3)_6]^{3+}$ or methylene blue with $[Fe(CN)_6]^{3-}$ system were previously described.[27–30] We considered miR-21 as a model target to test the applicability of our assay both in synthetic and biological samples, which was reported to have a strong correlation with the progression of ovarian cancer.[2] Our assay enables a highly sensitive detection limit of 1.0 fM and 10 cells in the synthetic and ovarian cancer cell line population, respectively.

2. Results and Discussion

The surface morphology of the samples before and after the calcination was observed by SEM (Figure 1A). The detailed synthetic procedures are described in the Supporting Information. The original 2D morphology of the GO sheets is well-preserved even after calcination. In the case of the GO/IO hybrid samples, the surface of GO is homogeneously covered

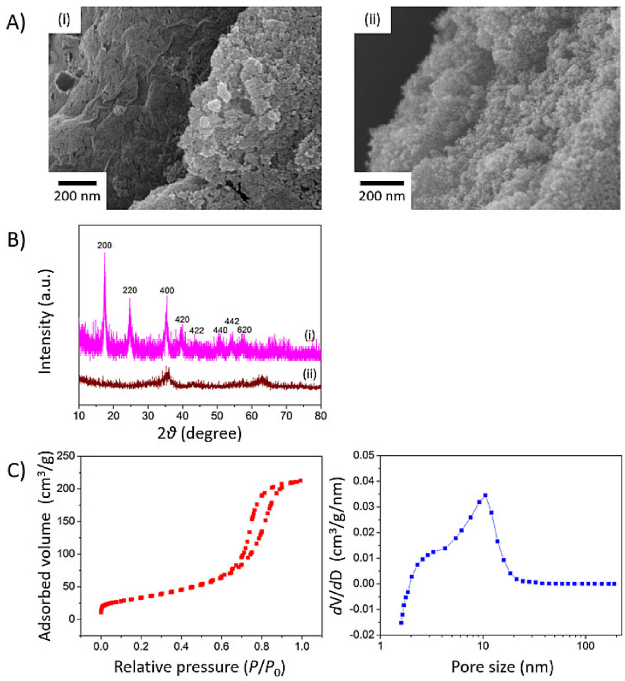

Figure 1. A) SEM images of samples prepared with GO/PB = 25:75 i) before and ii) after calcination. B) Wide-angle XRD patterns of samples prepared with GO/PB = 25:75 i) before and ii) after calcination. C) N_2 adsorption–desorption isotherm and pore-size distribution of GO/IO sample prepared with GO/PB = 25:75.

with fine IO nanoparticles. To carefully investigate the crystal structure and the phase purity of the samples before and after calcination, wide-angle XRD measurement was carried out (Figure 1B). In general, GO sheets themselves display a strong peak at around 10° and 26° which can be assigned to the interlayer spacing between the GO sheets. After hybridization with the Prussian blue (PB) nanoparticles, however, the diffraction peak derived from the GO sheets disappeared, while several new intense reflections corresponding to PB could be observed (JCPDF no. 01-070-0557). This indicates that the PB nanoparticles are located within the stacked GO sheets interlayer spacing which becomes disordered. The optimal calcination resulted in the formation of an impurity-free γ-Fe_2O_3 phase in the resulting hybrid materials, as identified from the XRD peaks at around 35° and 63°. To evaluate the surface area and porosity of the GO/IO hybrids, N_2 adsorption-desorption isotherms were carried out (Figure 1C). The surface areas and the pore volumes were calculated to be 120.5 $m^2 g^{-1}$ and 0.384 $cm^3 g^{-1}$ by the Brunauer-Emmett-Teller (BET) method and Barrett-Joyner-Halenda (BJH) method, respectively. The main pore size was estimated to be around 10 nm. This formation is attributed to the GO/IO interlayer space and/or the IO interparticle space.

To demonstrate the electrocatalytic activity of GO/IO hybrids, the cyclic voltammetric (CV) measurements of GO/IO hybrid-modified glassy carbon electrode (GCE) were carried out in the presence $[Ru(NH_3)_6]^{3+/2+}$. As shown in Figure 2A, well-defined cathodic and anodic peaks for the $[Ru(NH_3)_6]^{3+/2+}$ system were attained at −250 mV and −180 mV (vs. Ag/AgCl) respectively at the unmodified GCE (GCE/bare). This demonstrates the occurrence of single electron reversible process (ΔE = 70 mV). However, GO/IO hybrid material-modified GCE shows an enhanced cathodic and anodic peak current with higher peak separation compared to those of bare (Figure 2A). It can be seen that GCE/GO-IO hybrid material i_{pc} (cathodic current) increased approximately 3.5-times (10.9 vs. 36.62 μA cm^{-2}) with E_{pc} (cathodic potential) shifted by −77 mV, whereas i_{pa} (anodic current) increased approximately two-times (6.08 vs. 13.93 μA cm^{-2}) with an E_{pa} (anodic potential) shift of ~ −24 mV. These data indicate that GO/IO hybrid samples catalyzed both the oxidation and reduction of RuHex where the catalytic reduction was relatively faster. It is believed that the enhanced peak separation at GCE/GO-IO hybrid material is attributed to an enhanced electrocatalytic activity resulting from the intrinsic functionalities of Fe_3O_4.[24]

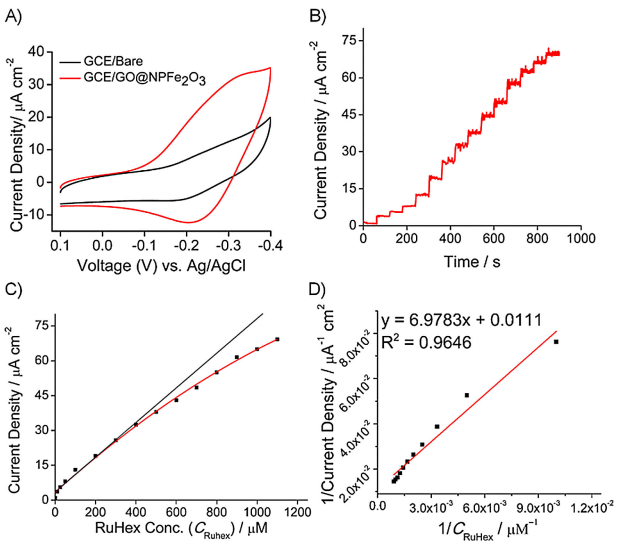

Figure 2. A) Comparison of the CVs obtained at an unmodified GCE and GO/IO-modified GCE in 50 mM RuHex (scan rate, 50 mV s^{-1}); B) amperometric responses of GCE/GO-IO material with the successive addition of RuHex solution (10 to 1100 μM) into 0.01 M PBS (pH-7); C) the corresponding calibration plot (red) that follows typical Michaelis–Menten equation for enzyme catalysis; and D) the electrochemical version of Lineweaver–Burk Model.

To understand the charge transport mechanism, we recorded CVs of both GCE/bare and GCE/GO-IO hybrid as a function of scan rates (10–1500 mV s^{-1}). As shown in Figure S1A (Supporting Information), both the i_{pc} and i_{pa} increase with an increasing scan rate spanning from 10 to 1500 mV s^{-1}, indicating the stable electrocatalytic activity of GO/IO hybrid materials within the applied range of scan rates. This is one of the characteristic features of a reversible redox reaction. Figure S1B shows a linear relationship between i_{pc} and i_{pa} with the square root of the scan rate for both the unmodified and modified GCE. This observation suggests that the electrocatalytic redox reactions of RuHex at the GCE/GO-IO hybrid electrode occurred mainly through the diffusion-limited process. Figure S1B also shows that the curve of i_{pc} and i_{pa} versus square root of the scan rate for the GCE/GO/IO hybrid electrode resulted in a steeper slope than that of the unmodified GCE. This further confirms the relatively high catalytic activity of GO/IO hybrid materials towards the redox reaction of RuHex.

To further examine the electrocatalytic activity of GO/IO hybrid materials, chronoamperometric (CA) readout was obtained at the GCE/GO-IO hybrid electrode with the successive addition of RuHex. As can be seen in Figure 2B and C, with the increase of RuHex concentration, after an initial increase in the CA current response, the current reached a plateau suggesting the saturation of RuHex. The second order exponential calibration curve (red) shown here clearly follows typical Michaelis–Menten equation for enzyme catalysis.[31] The apparent Michaelis–Menten constant (K_m^{app}) obtained from the electrochemical version of Lineweaver–Burk[32] model (Figure 2D) was estimated to be 0.64 mM. It is important to mention that Km^{app} herein denotes the concentration of RuHex that is required to reach the half of maximum current response (I_{max}) value, thus Km^{app} can be considered as an indicator of the GO/IO hybrid nanomaterials' affinity towards RuHex. This significantly low value of Km^{app} value suggests an increased affinity of GO/IO to RuHex, which also verifies the high electrocatalytic activity of GO/IO hybrid material towards the reduction of RuHex.

Figure 3 represents the outline of miRNA detection assay. In the assay, magnetically captured and purified target miR-21 was directly adsorbed on the GO/IO hybrids- modified screen-printed carbon electrode (SPCE) surface followed by a CC readout using $[Ru(NH_3)_6]^{3+}/[Fe(CN)_6]^{3-}$ electrocatalytic cycle. Briefly, total RNA was extracted and purified from cell lines. RNA

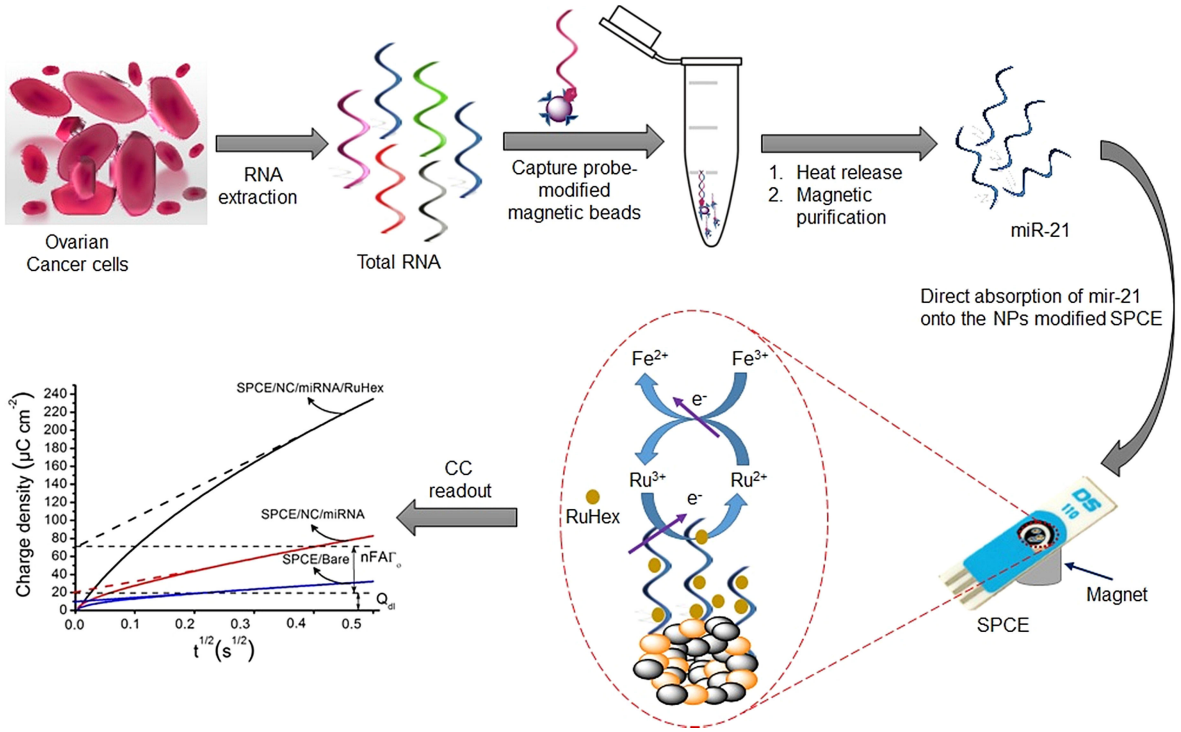

Figure 3. Schematic of the quantification of miRNA assay. Magnetically purified and separated miRNA from the extracted RNA sample pool were adsorbed directly on the magnetically bound GO/IO- modified SPCE. A significant electrocatalytic signal amplification was achieved through the chronocoulometric (CC) charge interrogation of target miRNA-bound $[Ru(NH_3)_6]^{3+}$–$[Fe(CN)_6]^{3-}$ electrocatalytic assay system.

sample was then incubated with miR-21 specific biotinylated capture probe for hybridization. Following target hybridization, streptavidin-labelled dynabeads were dispersed into the sample containing hybridized targets to purify and capture the target analyte *via* dynabead-based standard separation protocol. The heat-released target miRNA was isolated by another magnetic separation step (See experimental for details) and directly adsorbed onto the GO/IO- modified SPCE using RNA- graphene oxide (GO) affinity interaction. We and others previously demonstrated a number of bioassays which rely on nucleic acid-gold affinity interaction.[33–38] Similar to the nucleic acid-gold affinity interaction, direct physisorption of nucleotides (DNA/RNA) on graphene surface has been reported to be influenced by the polarizabilities of the individual nucleobases, where van der Wall (vdW) is considered to be the driving force for the adsorption process.[39,40] A number of studies also showed that the adsorption of nucleic acids on GO surface is influenced by π–π stacking, hydrophobic interaction and hydrogen bonding, and proposed Langmuir–Hinshelwood and Eley–Rideal mechanism could be responsible for this interaction.[41–43] The target miR-21 was then quantified by CC charge interrogation via measuring the saturated amount of charge-compensating $[Ru(NH_3)_6]^{3+}$ molecules, where positively charged $[Ru(NH_3)_6]^{4+/3+}$ stoichiometrically binds to the negatively charged phosphate backbone of miRNA adsorbed on the SPCE/GO-IO surface. To generate a high electrocatalytic signal amplification, $[Ru(NH_3)_6]^{3+}$ system was coupled to $[Fe(CN)_6]^{3-}$ system. $[Fe(CN)_6]^{3-}$ in the solution-phase further triggers the electrocatalytic reduction of $[Ru(NH_3)_6]^{3+}$. Since the $[Fe(CN)_6]^{3-}$ is a relatively stronger oxidant, it oxidized $[Ru(NH_3)_6]^{2+}$ for the regeneration of $[Ru(NH_3)_6]^{3+}$ allowing multiple turnovers of $[Ru(NH_3)_6]^{3+}$ resulting in a drastic increase in the signal. Thus, the amount of CC charge generated by $[Ru(NH_3)_6]^{3+}$ and $[Fe(CN)_6]^{3-}$ system should have a clear correlation with the concentration of miRNA.

To assess the analytical functionality and specificity of our assay, we investigated a number of control experiments with 100 pM of starting synthetic RNA using i) sensor modified with GO/IO hybrid materials and IO (i.e. nanoporous iron oxide without GO); ii) with ($[Ru(NH_3)_6]^{3+}$/$[Fe(CN)_6]^{3-}$ system) and without electrocatalytic cycle (only $[Ru(NH_3)_6]^{3+}$ system); and iii) closely-related non-targets (wrong targets) and no-template (NoT) controls. As shown in Figure 4A (left bar), the total charge density (both the Faradaic and non-Faradaic charges) obtained with Fe_2O_3 modified (i.e. SPCE/IO) sensor gives a little response in CC data (4.5 μC cm^{-2}). It was expected that in the absence of GO that acted as a platform carrier for RNA molecules in our assay, target miRNA would not be adsorbed on the SPCE/IO surface. As the CC response depends on the amount of target miRNA bound with $[Ru(NH_3)_6]^{3+}$ molecules, SPCE/IO gives an expected negligible response. However, this response is slightly higher than that found with bare SPCE (Figure S2, left bar, 4.5 versus 1.7 μC cm^{-2}) and may be comprised of both the Faradaic and non-Faradaic component of the charges, where Faradaic response could be related to the possibility of non-specific adsorption of a very tiny amount of redox active $[Ru(NH_3)_6]^{3+}$ on the IO.

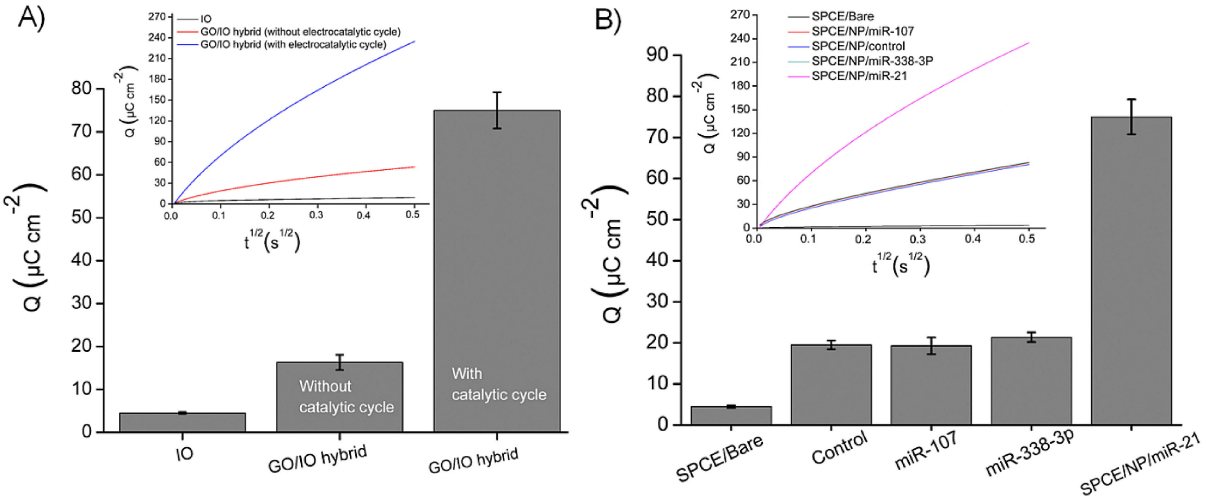

Figure 4. A) Corresponding charge density data with SPCE/Fe_2O_3, SPCE/GO-IO hybrid material (without electrocatalytic cycle), SPCE/GO-IO hybrid material (with electrocatalytic cycle) electrodes (total charge Q = faradic + non-faradic charges of the system); inset, corresponding CC curves (Q vs. $t^{1/2}$). B) Specificity of the assay. Corresponding charge density data of electrocatalytic cycle for the SPCE/Bare, control, non-complementary miR-107 and miR-338-3p, target miR-21; inset, corresponding CC curves (Q vs. $t^{1/2}$). Each data point represents the average of three independent trials, and error bars represent the standard deviation of measurements (% RSD = < 5 %, for n = 3).

When we performed the assay with GO/IO- modified SPCE in $[Ru(NH_3)_6]^{3+}$ system (Figure 4A, middle bar), a large increase in the total charge density was observed. This response was ~9 and ~3.6-folds higher, respectively, than those obtained with bare and IO- modified sensors (16.3 vs. 1.8 and 4.5 μC cm^{-2}). One of the reasons for this increased response is the large functional surface area of nanoporous GO/IO hybrid materials which can facilitate increased loading of target miRNA molecules. As demonstrated earlier, the intrinsic electrocatalytic activity of GO/IO hybrids towards the reduction of $[Ru(NH_3)_6]^{3+}$ is also a strong contributor to this higher CC charge response. To further enhance the catalytic signal, we coupled $[Fe(CN)_6]^{3-/4-}$ system with the $[Ru(NH_3)_6]^{3+/4+}$, which initiated the electrocatalytic cycle. As can be seen in the Figure 4A (right bar), the coupled system provides a significant enhancement in the charge response. This response is ~4.6-times higher than the response obtained with $[Ru(NH3)_6]^{3+/4+}$ system alone (Figure 4A, 75 vs. 16.3 μC cm^{-2}), which demonstrates the superior signal enhancement capacity of the electrocatalytic cycle (i.e., $[Ru(NH_3)_6]^{3+}$/$[Fe(CN)_6]^{3-}$ system) in our assay. This can be explained by the fact that the relatively stronger oxidant $[Fe(CN)_6]^{3-}$ electrocatalytically reduce the surface confined $[Ru(NH_3)_6]^{3+}$ in the solution phase, and initiates a cycle of redox reaction between $[Ru(NH_3)_6]^{3+}$ and $[Fe(CN)_6]^{3-}$, thereby increasing the rate of electron transfer.

To check the assay specificity, we performed our assay using control (SPCE/NP/NoT, no-template control) and non-complementary wrong sequences (synthetic miR-107 and miR-338–3p) with $[Ru(NH_3)_6]^{3+}$/$[Fe(CN)_6]^{3-}$ system. Figure 4B (two bars from left) shows that compared to the bare electrode, control gave an enlarged CC response. We predicted that due to the non-specific adsorption of a small number of $[Ru(NH_3)_6]^{3+}$ molecules on the enormous functional area of GO/IO hybrid materials, this charge response (19.5 μC cm^{-2}) was observed. However, this has not clearly affected the assay because almost an identical level of CC charge was counted for the two other unrelated miRNAs such as miR-107 (19.3 μC cm^{-2}) and miR-338-3p (21.4 μC cm^{-2}) (Figure 4B). While comparing the charge density responses obtained with control and non-targets with that resulting from target miR-21 (Figure 4B, right bar), a significant increase in the total charge density was observed (19.5/19.3/21.4 vs. 75 μC cm^{-2}). This demonstrates that our assay has high specificity and can detect the target RNA sequences in the background of closely related non-complementary non-target RNAs. It is worth noting that, expectedly a higher level of signal enhancement was observed with the electrocatalytic system (NoT vs target, 19.5 vs 75 μC cm^{-2}, Figure 4B) compared to that of the assay without electrocatalytic cycle (i.e., only $[Ru(NH_3)_6]^{3+}$ was present) (control vs target, 6.9 vs 16.3 μC cm^{-2}, Figure S2 and S3).

The sensitivity of the assay was evaluated by detecting a designated concentration of synthetic miR-21 spanning from 1.0 fM to 1.0 nM. As presented in Figure 5A and B, the total redox CC charge was increased with an increased concentration of target miR-21 using $[Ru(NH_3)_6]^{3+}$-$[Fe(CN)_6]^{3-}$ electrocatalytic cycle. Because with an increasing concentration of miRNA on the surface of GO/IO hybrid, an increasing number of cationic $[Ru(NH_3)_6]^{3+}$ will bind with the anionic backbone of the miRNAs. This results in an enhanced charge response in the $[Ru(NH_3)_6]^{3+}$-$[Fe(CN)_6]^{3-}$ electrocatalytic cycle. When we plot the concentration of RNA with the charge of RuHex (Q_{RNA}) electrostatically bound with target RNA (Figure 5B), the linear regression equation of the assay was estimated to be y (charge density, μC cm^{-2}) = 8.7246 (amount of miR-21) + 2.3519, with a correlation coefficient (R^2) of 0.9633. This clearly shows the wide dynamic range of our assay, and the limit of detection (LOD) was estimated to be 1.0 fM. This LOD, which is clearly distinguishable from that of control and bare electrodes with a high signal to noise ratio (i.e., 5:1), is comparable or better than most of the existing electrochemical miRNA biosensors.[7,26] We believe that the enormous functional area, and enhanced

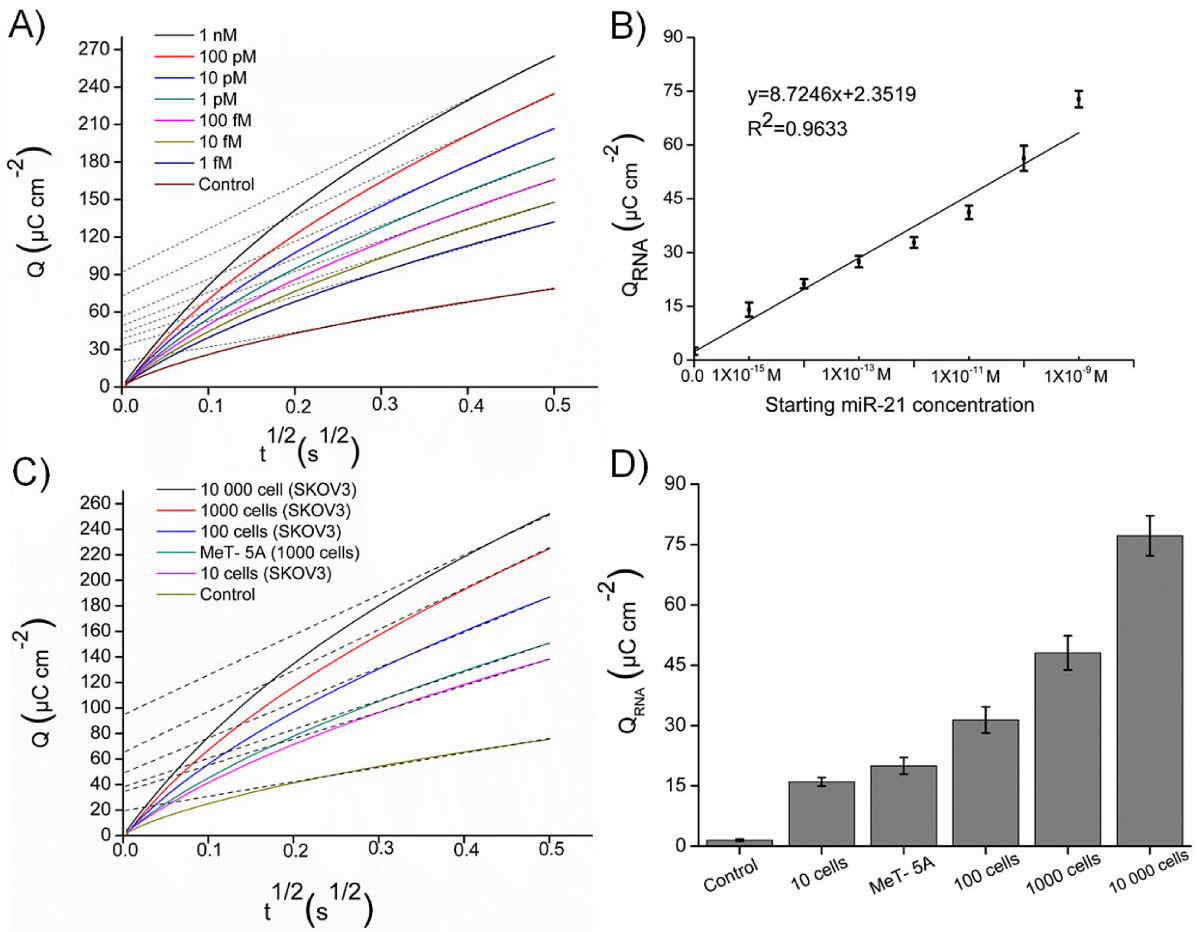

Figure 5. A) Typical CC curves (Q vs. $t^{1/2}$) for the SPCE/control and a designated concentration of synthetic miR21 (1.0 fM–1.0 nM). B) Corresponding calibration plot of Q_{RNA}-concentration profile across the range of 1.0 fM to 1.0 nM miR-21. C) Typical CC curves (Q vs. $t^{1/2}$) for the control and total RNA extracted from a known number of ovarian cancer SKOV3 (10, 100, 1000, 10 000 cells) and non-malignant MeT-5A (1000 cells) cell lines. D) Corresponding bar diagram of Q_{RNA}; Q_{RNA} (corresponding charge of target miRNA bound to surface bound RuHex) = total charge – capacitive charge. Each data point represents the average of three independent trials, and error bars represent the standard deviation of measurements (% RSD = < 5 %, for $n = 3$).

electrocatalytic activity of GO/IO hybrid materials, followed by the coupling of $[Fe(CN)_6]^{3-}$ (i.e., electrocatalytic cycle) system that facilitates an increased rate of electron transfer in the system, have attributed to this low LOD. Our observation was further confirmed when we compared the data with those obtained with the assay performed with $[Ru(NH_3)_6]^{3+}$ system alone (without the catalytic cycle step), where a thousand-fold less LOD was observed (1.0 fM versus 1.0 pM) (Figure 5A, B vs S3). It is noteworthy that despite attaining such high sensitivity and selectivity, we designed an inexpensive and straightforward assay compared to several reported electrochemical methods. Most of these methods rely on some forms of enzymatic amplification processes which complicate the assay. For example, Fang et al. reported an electrochemical assay with a similar detection limit of 2.0 fM. However, this method relies on the use of zinc finger protein and alkaline phosphatase-based enzymatic amplification.[44] Another electrochemical miR-21 sensor reported to have a detection limit of 5.36 fM, also relies on a complex arched probe mediated isothermal exponential amplification reaction.[45] Our method has achieved several hundred folds better sensitivity compared to a recent CC assay reported by Yao et al.[46] which also depends on enzyme-based rolling-circle amplification process. Compared to another recent voltammetric approach, we achieved 10-folds better sensitivity.[38] This approach also relies on enzymatic polyadenylation of the target miRNA. In comparison with aforementioned assays, we have not only attained better sensitivity but also avoid the possibility of miRNA degradation (due to target modification) and amplification bias.

To check the applicability of our assay in real samples, we performed our assay on total RNA isolated from designated numbers of ovarian cancer (SKOV3) and normal non-cancerous (MeT-5A) cell lines. Figure 5C and D show that SKOV3 cells (0, 10, 100, 1000, and 10 000 cells) lead to a gradually elevated charge density profile across the range of 0–10 000 cells. From the electrochemical response, it is evident that our assay can detect miR-21 from only a few numbers of cells (0–10 cells). As expected when we analyzed our assay in the non-cancerous MeT-5A (1000 cells), we found that the charge density profile is decreased which is close to that obtained with 10 SKOV3 cells (20.3 vs 16.1 $\mu C\,cm^{-2}$) (Figure 5D). Whereas, RNA derived from a similar number of SKOV3 cells (i.e., 1000 cells) gave a ~2.5

times higher chronocoulometric response (20.3 vs 48.1 μC cm^{-2}). This indicates that miR-21 is overexpressed in the tested SKOV3 cell lines compared to the non-cancerous cells. This preliminary data on cell lines indicate that our method retains its efficiency and sensitivity in analyzing miRNA from a complex sample, and may become useful in clinical analysis.

The acceptable range of our assay reproducibility (%RSD = < 5%, for $n = 3$) is also comparable or better than most of the existing electrochemical miRNA sensors.[6] There are several other distinct advantages of our assay. The major development is the utilization of high porosity and catalytic activities of a novel GO/IO hybrid nanomaterials that enables significantly increased loading of RNA samples and subsequent signal enhancement in the readout signal. This alternative signal amplification approach allows us to avoid any form of enzymatic amplification of the target. Another useful aspect of our assay is that we isolate miRNA by magnetic mixing and purification, which may lessen the matrix effects of the biological samples and thus, the assay is less prone to non-specific detection. Moreover, the nanoparticle modified electrodes provide a three dimensional surface for a large amount of target miRNA to diffuse with enhanced kinetics compared to the conventional electrodes. Our assay also uses a single-use (i.e., disposable) and relatively inexpensive SPCE which assists us to avoid the use of conventional disk electrodes, thus the assay is not affected with non-specific response resulting from the multiple surface reactions and excessive capacitive charges of disk electrodes. The elimination of tedious cleaning procedures of disk electrodes also reduces the assay time. Moreover, the direct adsorption of target miRNA on a GO/IO-modified electrode rather than the conventional hybridization-based approach of using recognition and transduction layers allows us to avoid complex conjugation chemistries of sensor fabrication. The overall features of this electrochemical sensor indicate that the assay can complement with the miniaturized, multiplexed and decentralized analysis of RNA biomarkers with high translational potential.

3. Conclusions

We presented the electrocatalytic activity of a new class of GO/IO hybrid nanomaterials for the development of a highly sensitive (LOD = 1.0 fM) and specific detection platform of miRNA. SPCEs modified with this novel material were used as a platform to adsorb magnetically isolated and purified target miRNA via graphene -RNA affinity interaction. The chronocoulometric signal of surface confined RuHex attached with adsorbed target miRNA was significantly enhanced when the system was coupled with a solution-borne ferricyanide system. The assay also showed excellent reproducibility (%RSD = < 5%, for $n = 3$) and specificity (highly selective against closely related non-target) while detecting miR-21 from cancer cells. We envisage that our assay would be potentially useful for ultrasensitive analysis of miRNA in biomedical research, and clinical diagnosis that further can potentially be extended to detect other clinically relevant nucleic acid biomarkers by simply choosing the respective capture probe.

Experimental Section

Isolation of Target miRNA

Total RNA was extracted from SKOV3 ovarian cancer and MeT-5A non-cancerous cell lines using **RNeasy Mini Kit** (Qiagen, Germany). Target miRNAs were hybridized with a complementary capture probe followed by magnetic bead based isolation and purifications. Target miRNAs were then heat-released from magnetic bead bound hybrid and resuspended in RNase-free water and stored at −20 °C for subsequent experiments (for details, see Supporting Information).

Evaluation of Electrocatalytic Activity of GO/IO Hybrid Materials

To evaluate the electrocatalytic activity of GO/IO hybrids, GO/IO hybrids were drop-dried onto the surface of a glassy carbon electrode (GCE). Cyclic voltammetry (CV) was carried out in the presence of a redox marker, RuHex, over the scan rates of 10–1500 mV s^{-1}. The chronoamperometric (CA) responses were measured at the GCE/GO/IO hybrid electrode at −0.25 V vs Ag/AgCl with the successive addition of RuHex (ranging from 10–1100 μM). The apparent Michaelis-Menten constant (K_m^{app}) of GCE/GO-IO hybrids was determined using the Michaelis-Menten equation and the electrochemical version of Lineweaver–Burk equation.[31,32] (See Supporting Information for electrode fabrication protocol and kinetic parameters calculations)

Electrochemical Detection of Target miR-21

For the CC detection of target miRNA, GO/IO hybrid materials were magnetically bound onto a SPCE using a permanent magnet. Magnetically purified miR-21 was then directly put onto that GO/IO hybrids followed by an incubation with RuHex so that positively charged Ru^{3+} can bind with the negatively charged phosphate backbone of electrode-bound miRNAs. The charge associated with the electrode-bound miRNAs was measured by CC in 40 mM Tris buffer (pH 7.4). The number of cationic redox molecules electrostatically associated with the surface-attached miRNA was calculated using integrated Cottrell equation (See details in Supporting Information).[47]

Acknowledgements

This work was supported by the NHMRC CDF (APP1088966 to M.J.A.S.), and higher degree research scholarships (GUIPRS and GUPRS scholarships to M.N.I and L.G) from the Griffith University.

Conflict of Interest

The authors declare no conflict of interest.

Keywords: microRNA detection · electrochemical detection · graphene oxide/iron oxide hybrid · electrocatalysis · ovarian cancer · screen-printed electrodes

[1] D. P. Bartel, *Cell* **2004**, *116*, 281–297.
[2] J. Wang, J. Chen, S. Sen, *J. Cell. Physiol.* **2016**, *231*, 25–30.
[3] M. N. Islam, M. K. Masud, M. H. Haque, M. S. A. Hossain, Y. Yamauchi, N.-T. Nguyen, M. J. A. Shiddiky, *Small Methods* **2017**, *1*, 1700131.
[4] P. Mestdagh, N. Hartmann, L. Baeriswyl, D. Andreasen, N. Bernard, C. Chen, D. Cheo, P. D'Andrade, M. DeMayo, L. Dennis, S. Derveaux, Y. Feng, S. Fulmer-Smentek, B. Gerstmayer, J. Gouffon, C. Grimley, E. Lader, K. Y. Lee, S. Luo, P. Mouritzen, A. Narayanan, S. Patel, S. Peiffer, S. Ruberg, G. Schroth, D. Schuster, J. M. Shaffer, E. J. Shelton, S. Silveria, U. Ulmanella, V. Veeramachaneni, F. Staedtler, T. Peters, T. Guettouche, L. Wong, J. Vandesompele, *Nat. Methods* **2014**, *11*, 809–815.
[5] T. Kilic, A. Erdem, M. Ozsoz, S. Carrara, *Biosens. Bioelectron.* **2018**, *99*, 525–546.
[6] M. Labib, E. H. Sargent, S. O. Kelley, *Chem. Rev.* **2016**.
[7] M. Labib, M. V. Berezovski, *Biosens. Bioelectron.* **2015**, *68*, 83–94.
[8] C. Zhu, G. Yang, H. Li, D. Du, Y. Lin, *Anal. Chem.* **2015**, *87*, 230–249.
[9] Y. Pang, C. Wang, J. Wang, Z. Sun, R. Xiao, S. Wang, *Biosens. Bioelectron.* **2016**, *79*, 574–580.
[10] S. C. McBain, H. H. P. Yiu, J. Dobson, *Int. J. Nanomed.* **2008**, *3*, 169–180.
[11] V. Urbanova, M. Magro, A. Gedanken, D. Baratella, F. Vianello, R. Zboril, *Chem. Mater.* **2014**, *26*, 6653–6673.
[12] F.-K. Shieh, S.-C. Wang, C.-I. Yen, C.-C. Wu, S. Dutta, L.-Y. Chou, J. V. Morabito, P. Hu, M.-H. Hsu, K. C. -W. Wu, C.-K. Tsung, *J. Am. Chem. Soc.* **2015**, *137*, 4276–4279.
[13] Y.-P. Wang, Y.-T. Liao, C.-H. Liu, J. Yu, H. R. Alamri, Z. A. Alothman, M. S. A. Hossain, Y. Yamauchi, K. C. -W. Wu, *ACS Biomater. Sci. Eng.* **2017**, *3*, 2366–2374.
[14] S.-H. Liao, C.-H. Liu, B. P. Bastakoti, N. Suzuki, Y. Chang, Y. Yamauchi, F.-H. Lin, K. C. -W. Wu, *Int. J. Nanomed.* **2015**, *10*, 3315–3328.
[15] C. Ya-Dong, D. Saikat, C. Ching-Tien, H. Yu-Tzu, L. Kuen-Song, W. J. C. S. , S. Norihiro, Y. Yusuke, K. C.-W. Wu, *ChemSusChem*, **2015**, *8*, 789–794.
[16] L. Yi-Chun, C. Ching-Tien, C. Yu-Ting, K. C.-W. Wu, *ChemCatChem*, **2013**, *5*, 2153–2157.
[17] C. He, D. Liu, W. Lin, *Chem. Rev.* **2015**, *115*, 11079–11108.
[18] A. Katsuhiko, V. Ajayan, Y. Yusuke, J. Qingmin, *Bull. Chem. Soc. Jpn.* **2012**, *85*, 1–32.
[19] K. C.-F. Leung, S. Xuan, X. Zhu, D. Wang, C.-P. Chak, S.-F. Lee, W. K. W. Ho, B. C. T. Chung, *Chem. Soc. Rev.* **2012**, *41*, 1911–1928.
[20] S. Yadav, M. K. Masud, M. N. Islam, V. Gopalan, A. K. Lam, S. Tanaka, N.-T. Nguyen, M. S. Hossain, C. Li, Y. Yamauchi, M. J. A. Shiddiky, *Nanoscale* **2017**, *9*, 8805–8814
[21] S. Tanaka, R. R. Salunkhe, Y. V. Kaneti, V. Malgras, S. M. Alshehri, T. Ahamad, M. B. Zakaria, S. X. Dou, Y. Yamauchi, M. S. A. Hossain, *RSC Adv.* **2017**, *7*, 33994–33999.
[22] M. N. Islam, M. K. Masud, N.-T. Nguyen, V. Gopalan, H. R. Alamri, Z. A. Alothman, M. S. A. Hossain, Y. Yamauchi, A. K.-Y. Lam, M. J. A. Shiddiky, *Biosens. Bioelectron.* **2018**, *101*, 275–281.
[23] M. K. Masud, S. Yadav, M. N. Islam, N.-T. Nguyen, C. Salomon, R. Kline, H. R. Alamri, Z. A. Alothman, Y. Yamauchi, M. S. A. Hossain, M. J. A. Shiddiky, *Anal. Chem.* **2017**, *89*, 11005–11013.
[24] M. K. Masud, M. N. Islam, M. H. Haque, S. Tanaka, V. Gopalan, G. Alici, N.-T. Nguyen, A. K. Lam, M. S. A. Hossain, Y. Yamauchi, M. J. A. Shiddiky, *Chem. Commun.* **2017**, *53*, 8231–8234.
[25] J. Kim, S.-J. Park, D.-H. Min, *Anal. Chem.* **2017**, *89*, 232–248.
[26] Y. Fang, E. Wang, *Chem. Commun.* **2013**, *49*, 9526–9539.
[27] J. Zhang, L. Wang, D. Pan, S. Song, C. Fan, *Chem. Commun.* **2007**, 1154–1156.
[28] R. Gasparac, B. J. Taft, M. A. Lapierre-Devlin, A. D. Lazareck, J. M. Xu, S. O. Kelley, *J. Am. Chem. Soc.* **2004**, *126*, 12270–12271.
[29] E. M. Boon, D. M. Ceres, T. G. Drummond, M. G. Hill, J. K. Barton, *Nat. Biotechnol.* **2000**, *18*, 1096–1100.
[30] S. O. Kelley, E. M. Boon, J. K. Barton, N. M. Jackson, M. G. Hill, *Nucleic Acids Res.* **1999**, *27*, 4830–4837.
[31] L. Lehninger, D. L. Nelson, M. M. Cox, *Lehninger Principles of Biochemistry*. W. H.Freeman & Co Ltd: New York, **2005**.
[32] H. Lineweaver, D. Burk, *J. Am. Chem. Soc.* **1934**, *56*, 658–666.
[33] M. N. Islam, V. Gopalan, M. H. Haque, M. K. Masud, M. S. A. Hossain, Y. Yamauchi, N.-T. Nguyen, A. K.-Y. Lam, M. J. A. Shiddiky, *Biosens. Bioelectron.* **2017**, *98*, 227–233.
[34] M. N. Islam, S. Yadav, M. Hakimul Haque, A. Munaz, F. Islam, M. S. Al Hossain, V. Gopalan, A. K. Lam, N.-T. Nguyen, M. J. A. Shiddiky, *Biosens. Bioelectron.* **2017**, *92*, 668–678.
[35] K. Boriachek, M. Umer, M. N. Islam, V. Gopalan, A. K. Lam, N.-T. Nguyen, M. J. A. Shiddiky, *Analyst* **2018**.
[36] T. Hossain, G. Mahmudunnabi, M. K. Masud, M. N. Islam, L. Ooi, K. Konstantinov, M. S. A. Hossain, B. Martinac, G. Alici, N.-T. Nguyen, M. J. A. Shiddiky, *Biosens. Bioelectron.* **2017**, *94*, 63–73.
[37] K. M. Koo, A. A. I. Sina, L. G. Carrascosa, M. J. A. Shiddiky, M. Trau, *Anal. Methods* **2015**, *7*, 7042–7054.
[38] K. M. Koo, L. G. Carrascosa, M. J. Shiddiky, M. Trau, *Anal. Chem.* **2016**, *88*, 2000–2005.
[39] M. H. Haque, V. Gopalan, S. Yadav, M. N. Islam, E. Eftekhari, Q. Li, L. G. Carrascosa, N.-T. Nguyen, A. K. Lam, M. J. A. Shiddiky, *Biosens. Bioelectron.* **2017**, *87*, 615–621.
[40] S. Gowtham, R. H. Scheicher, R. Ahuja, R. Pandey, S. P. Karna, *Phys. Rev. B* **2007**, *76*, 033401.
[41] S. Manohar, A. R. Mantz, K. E. Bancroft, C.-Y. Hui, A. Jagota, D. V. Vezenov, *Nano Lett.* **2008**, *8*, 4365–4372.
[42] J. S. Park, H. K. Na, D. H. Min, D. E. Kim, *Analyst* **2013**, *138*, 1745–1749.
[43] P.-J. J. Huang, J. Liu, *Anal. Chem.* **2012**, *84*, 4192–4198.
[44] C. S. Fang, K.-s. Kim, B. Yu, S. Jon, M.-S. Kim, H. Yang, *Anal. Chem.* **2017**, *89*, 2024–2031.
[45] Y. Yu, Z. Chen, L. Shi, F. Yang, J. Pan, B. Zhang, D. Sun, *Anal. Chem.* **2014**, *86*, 8200–8205.
[46] B. Yao, Y. Liu, M. Tabata, H. Zhu, Y. Miyahara, *Chem. Commun.* **2014**, *50*, 9704–9706.
[47] A. B. Steel, T. M. Herne, M. J. Tarlov, *Anal. Chem.* **1998**, *70*, 4670–4677.

Manuscript received: March 13, 2018
Accepted Article published: June 12, 2018
Version of record online: June 27, 2018